Effects of three-dimensional slit geometry on flashback of premixed hydrogen flames in perforated burners

Filippo Fruzza[a], Hongchao Chu[b], Rachele Lamioni[a], Temistocle Grenga[c], Chiara Galletti[a], Heinz Pitsch[b]

[a]*Dipartimento di Ingegneria Civile e Industriale, Università di Pisa, 56122 Pisa, Italy*
[b]*Institute for Combustion Technology, RWTH Aachen University, Aachen 52056, Germany*
[c]*Faculty of Engineering and Physical Sciences, University of Southampton, Southampton SO17 1BJ, UK*

Abstract

Addressing flashback represents a pivotal challenge in the advancement of innovative perforated burners intended to substitute natural gas with hydrogen in household appliances. Current numerical models, employing 2D configurations to estimate flashback velocities in the slits of such burners, offer valuable insights with reasonable computational costs. However, the inherent complexity of the phenomena suggests that a 2D model may inadequately capture flashback dynamics, resulting in inaccurate estimations of flashback limits. In this study, 3D simulations are employed for the first time to explore the impact of the three-dimensional shape of slits on the flashback limits of hydrogen-premixed flames. Steady-state simulations are conducted to compute flashback limits for three equivalence ratios ($\phi = 0.6$, 0.8, and 1.0), investigating slits with fixed width and varying lengths up to $8\,\mathrm{mm}$. Additionally, transient simulations are performed to investigate the flash-

---

*Corresponding author
Email address:* `rachele.lamioni@unipi.it` (Rachele Lamioni)

back dynamics. The results are compared with those from 2D configurations to assess the reliability of the infinite slit approximation. Notably, 2D simulations significantly underestimate flashback limits as the critical initiation region is consistently located at the slit extremities, which are neglected in 2D configurations. For the same reason, the flashback velocity exhibits weak dependence on slit length, since the flashback is consistently initiated at the slit far ends regardless of length. The physical mechanisms driving the initiation of flashback in that zone are identified as preferential diffusion effects, which cause the enrichment of the mixture at the slit extremities, and enhanced heat transfer promoted by the enclosed geometry, which increases the pre-heating of the fresh gases in that regions. These findings underscore the necessity of taking into account three-dimensional effects in numerical simulations for accurate estimations of the flashback limits in domestic burners.

Keywords: Hydrogen, Flashback, Premixed flame, Perforated burner

1. Introduction

As Europe strives to meet the ambitious targets set by the EU Green Deal, the role of green hydrogen has garnered significant attention [1, 2]. One of its promising applications is in the decarbonization of heating for residential and commercial buildings, especially when the transition to electrification, is financially burdensome and technically complex, like in older buildings [3, 4]. These applications often rely on domestic end-user devices like condensing boilers equipped with perforated burners, which inject premixed fuel-air mixtures into combustion chambers, generating short-length flames that fit within the compact space between the burner and heat ex-

2

changer coils [5–9]. The introduction of hydrogen, either in its pure form or as a blend with natural gas, presents an opportunity for substantial emissions reduction [10–13].

However, the use of hydrogen as a fuel presents unique challenges due to its distinct physical properties compared to natural gas, which is currently the dominant fuel source for these devices. Its laminar flame speed is approximately six times higher than that of natural gas under stoichiometric conditions, and its flame thickness is much smaller. Furthermore, hydrogen exhibits a broader flammability range [14]. Hydrogen-air mixtures have a lower effective Lewis number, altering combustion characteristics and complicating the stabilization of premixed hydrogen flames, introducing thermo-diffusive instabilities [15]. Given that domestic burners typically operate in premixed conditions, understanding these effects is crucial in the design process to prevent safety issues and performance problems, such as elevated burner temperatures and flashback.

As a first approximation, the stabilization of premixed flames is primarily determined by the ratio of flame speed to bulk flow velocity. However, numerous distinct factors significantly contribute to flame stabilization, encompassing a range of phenomena such as flame-wall conjugate heat transfer, curvature, stretch rate, Soret diffusion, preferential diffusion effects, and interactions between the flame and the surrounding walls [16–21]. Notably, the influence of wall heat losses and wall temperatures has been emphasized in several studies [22–25]. Furthermore, the significance of flow-flame interactions in the dynamics of boundary-layer flashback, especially in hydrogen-enriched swirled flames, has been demonstrated in various investigations [26–

3

28].

Experimental examinations of flashback limits for H_2-enriched mixtures in domestic boilers have been undertaken in previous studies [29–31]. In parallel, numerical assessments conducted by Vance et al. [19, 32, 33] have explored the influence of parameters such as heat losses, stretch, Lewis number, and Soret diffusion on the stabilization of H_2-air and H_2-CH_4-air flames within 2D configurations. Similarly, 2D configurations have been employed in research by Fruzza et al. [34] and Flores-Montoya et al. [35], both of which investigated the flashback limits of H_2-enriched mixtures in multi-slit burners. These studies have collectively revealed two distinct flashback regimes contingent upon the hydrogen content. Recently, Fruzza et al. [36] have further explored this configuration, employing stochastic sensitivity analysis methods to investigate the relative impact of H_2 content, equivalence ratio, and geometrical parameters on the flashback limits of highly H_2-enriched lean flames.

However, the range of applicability of the infinite slit approximation, commonly assumed in 2D configurations, has not been verified in the literature. Moreover, the physical mechanisms governing the flashback of premixed hydrogen flames are likely influenced by three-dimensional effects. For instance, preferential diffusion is driven by curvature, a three-dimensional quantity. Therefore, 2D models may not accurately capture the actual flashback dynamics in a real burner, leading to inaccurate estimations of flashback velocities. In this study, we conduct, for the first time, numerical simulations in 3D configurations to explore the effect of the three-dimensional shape of the slit on the flashback limits of H_2-air flames. The numerical model incorpo-

rates conjugate heat transfer between the flame and the burner plate. We adopt a dual approach, using both steady-state simulations to investigate the effect of slit length over a wide range at different equivalence ratios and transient simulations to capture flashback dynamics. The results are then compared with those obtained in 2D configurations to assess the reliability of the infinite slit approximation.

2. Configuration and numerical methods

In this study, we simulate a segment of the perforated plate of a real burner plate typically used in domestic condensing boilers. 3D configurations representing arrays of holes or slits of different shapes and sizes are considered. The 3D configuration is shown in Figure 1 along with the computational domain. Due to the symmetries of the problem, the computational domain can be reduced to a quarter of the entire slit, with symmetry boundary conditions on the symmetry planes. The fluid domain extends enough both downstream ($H_{\text{out}} = 8\,\text{mm}$) and upstream ($H_{\text{in}} = 4\,\text{mm}$) of the solid. The slit width is denoted by W, while the distance between two adjacent slits is denoted by D. The distance between the centers of the round ends of the slit is represented by L, so that $L = 0\,\text{mm}$ corresponds to a circular hole of diameter W. The burner plate thickness is $T = 0.6\,\text{mm}$ for all cases, while the slit width remains fixed at $W = 0.5\,\text{mm}$. The slit length is varied within the range $L \in [0\,\text{mm} - 8\,\text{mm}]$, which covers a practical investigation range. For a given combination of the parameters W and L, the distance between slits D can be adjusted to fix the porosity of the burner, defined as $A_{\text{slit}}/A_{\text{tot}}$, where A_{slit} is the perforated area and A_{tot} is the sum of the plate
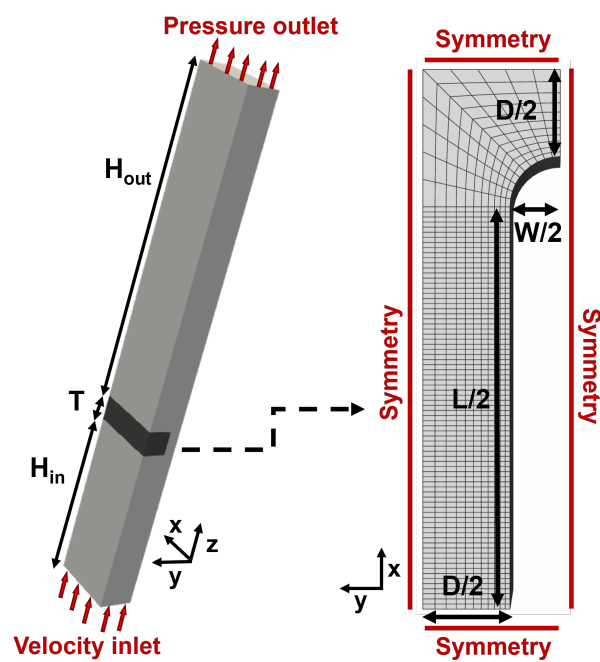
Figure 1: Left panel: computational domain (fluid zone in ligth gray, solid zone in dark grey). Bottom panel: slit geometry. Boundary conditions are indicated in red.

and the perforated areas. We use H_2-air mixtures at different equivalence ratios ϕ. Uniform velocity and uniform temperature of $T_u = 300\,\text{K}$ are set at the inlet, and a pressure outlet with $p = 1\,\text{atm}$ is imposed at the outlet. At the fluid-solid interface, a no-slip boundary condition is given for the velocity, and zero-mass flux is imposed for the species equations. No thermal boundary conditions are needed at the fluid-solid interface since the heat fluxes are computed directly as described below.

The transport equations of mass, momentum, energy, and mass fractions of chemical species are given as:

$$\frac{\partial \rho}{\partial t} + \nabla \cdot (\rho \mathbf{v}) = 0 \tag{1}$$

$$\frac{\partial}{\partial t} (\rho \mathbf{v}) + \nabla \cdot (\rho \mathbf{v} \mathbf{v}) = -\nabla p + \nabla \cdot (\bar{\tau}) \tag{2}$$

$$\frac{\partial}{\partial t} (\rho E) + \nabla \cdot (\mathbf{v} (\rho E + p)) =$$
$$= \nabla \cdot \left(k \nabla T + \sum_{j=1}^{N} h_j \left(\sum_{k=1}^{N-1} \rho D_{m,jk} \nabla Y_k + D_{T,j} \frac{\nabla T}{T} \right) \right) - \sum_{j=1}^{N} h_j \omega_j + S_{rad} \tag{3}$$

$$\frac{\partial}{\partial t} (\rho Y_i) + \nabla \cdot (\rho \mathbf{v} Y_i) = \nabla \cdot \left(\sum_{j=1}^{N-1} \rho D_{m,ij} \nabla Y_j + D_{T,i} \frac{\nabla T}{T} \right) + \omega_i, \tag{4}$$

where ρ is the density, $\mathbf{v}$ is the velocity vector, p is the pressure and $\bar{\tau}$ is the stress tensor. The gas phase is modeled as an ideal gas. T is the temperature, h_i, Y_i and ω_i are the enthalpy, the mass fraction, and the net rate of production of the ith species, respectively, and $E = \sum_{i=1}^{N} h_i Y_i - p/\rho + |\vec{v}|^2/2$. k is the mass-weighted thermal conductivity of the mixture, $D_{m,ij}$ are the generalized Fick's law diffusion coefficients of the species i in species j, and $D_{T,i}$ are the thermal diffusion coefficients of the ith species. Finally, S_{rad}

is the energy source associated with radiation. The burner plate is modeled as a solid with the properties of the stainless steel typically used for this kind of burner, with density $\rho_s = 7719\,\mathrm{kg\,m^{-3}}$, specific heat $c_{p,s} = 461.3\,\mathrm{J\,kg^{-1}\,K^{-1}}$, and thermal conductivity $k_s = 22.54\,\mathrm{W\,m^{-1}\,K^{-1}}$. Inside the solid domain, we solve the energy equation:

$$\frac{\partial}{\partial t}\left(\rho_s h_s\right) = \nabla \cdot \left(k_s \nabla T\right) \tag{5}$$

where $h_s = \int_{T_0}^{T} c_{p,s}\, dT$ is the sensible enthalpy of the solid material.

The equations are solved on a structured grid, with characteristic cell size in the reaction region of $\Delta x = 25\,\mathrm{\mu m} \simeq \delta_F/13$, where δ_F is the 1D unstretched flame thickness. The mesh is slightly stretched in both the x and y directions towards the domain boundaries and in the z direction towards the inlet and outlet, far from the reaction zone. We employ detailed chemistry, utilizing a reduced mechanism comprising 9 chemical species and 22 reactions. This reduced mechanism is derived from the Kee-58 skeletal mechanism [37]. This choice ensures consistency with prior research involving CH_4/H_2 mixtures up to 100% H_2, where the same mechanism was utilized [34, 36]. Full multi-component diffusion is modeled through generalized Fick's law coefficients derived by the Maxwell-Stefan equations [38–40]. Soret diffusion is modeled using the following empirically-based composition-dependent expression provided by Kuo [41]:

$$D_{T,i} = -2.59 \times 10^{-7} T^{0.659} \left[\frac{M_i^{0.511} X_i}{\sum_{j=1}^{N} M_j^{0.511} X_j} - Y_i\right] \cdot \left[\frac{\sum_{j=1}^{N} M_j^{0.511} X_j}{\sum_{j=1}^{N} M_j^{0.489} X_j}\right], \tag{6}$$

where M_i, X_i, and Y_i are the molar mass, molar fraction, and mass fraction, respectively, of the species i. Radiation is modeled by means of the gray

8

Discrete Ordinates (DO) method [42], assuming the emissivity of the fluid-solid interface to be 0.85. The conjugate heat transfer (CHT) between the fluid and the solid zones is modeled to consider the interaction between the flame and the burner plate. The CHT is modeled using Fourier's Law to compute the heat flux through the fluid-solid interface [38].

3. Solution methodology

We perform steady-state simulations using a pressure-based coupled algorithm [38] and a second-order scheme for spatial discretization. Given the large number of simulations required for the parametric variations investigated in this study, a steady-state approach is needed for reasons of computational cost. We start from a relatively high inlet velocity, ensuring a stable flame solution. The inlet velocity is then systematically reduced until the steady-state solver no longer converges to a stable flame solution, signifying the attainment of the critical inlet velocity for flashback. To accurately estimate this flashback inlet velocity, the minimum decrement of the inlet velocity is set at $\Delta V_{\text{in}} = 0.01\,\text{m/s}$, where V_{in} is the uniform inlet velocity. Neglecting the density variations of the mixture due to the high burner plate temperatures, the cold-flow bulk velocity at the slit entry is defined as

$$V_{\text{S}} = \frac{A_{\text{tot}}}{A_{\text{slit}}} V_{\text{in}}. \tag{7}$$

Following [33], the flashback velocity V_{FB} is defined as

$$V_{\text{FB}} = V_{\text{S}}|_{FB} = \frac{A_{\text{tot}}}{A_{\text{slit}}} V_{\text{in}}|_{FB}. \tag{8}$$

To validate the reliability of the steady-state approach, we perform transient simulations on a domain that encompasses the entire slit geometry,

9

rather than just a quarter. This is undertaken to capture potential asymmetries in flashback dynamics. The PISO implicit algorithm is employed [38], with a second-order scheme for time discretization. The solution methodology remains the same as described above, with a minimum velocity decrement of $\Delta V_{\text{in}} = 0.01\,\text{m/s}$. In the fluid domain, a time step of $\Delta t = 1\,\text{μs}$ is employed. However, the characteristic time scales of heat conduction within the solid domain are considerably higher. Consequently, implementing a uniform time step across the entire computational domain would require excessively long simulations for the burner temperature to stabilize, rendering it infeasible due to computational costs. To address this, a larger time step for the solid zone, $\Delta t_s = 10^3 \Delta t$, is applied. Similar methodologies have been previously applied in flashback simulations [34, 35]. It is worth noting that further reducing the solid time step does not change the estimated flashback velocities, but does impact the flashback dynamics: while effective for steady-state solutions, this approach has limitations during the flashback occurrence, as the artificially accelerated heating of the solid introduces unphysical flame oscillations. Therefore, once the flashback velocity is determined using this method, the final stage of the simulation, corresponding to the flashback occurrence, is repeated with a uniform time step of $\Delta t = 1\,\text{μs}$ in both phases. This ensures an accurate capture of the flashback dynamics without being influenced by the unphysical heating of the solid.

For transient simulations, two test cases were considered: a circular hole with a diameter of $W = 0.5\,\text{mm}$ and a slit with a width of $W = 0.5\,\text{mm}$ and length of $L = 2\,\text{mm}$, at an equivalence ratio of $\phi = 0.6$. The transient approach exhibited no significant discrepancies compared to the steady-state

method. Therefore, we opted for the faster steady-state approach to estimate flashback velocities across a broad range of geometrical and operational parameters. A more detailed comparison between the two approaches can be found in the Supplementary Material.

4. Results and discussion

4.1. Preliminary analysis

All previous numerical studies on flashback in multi-slit burners have been conducted using 2D configurations, corresponding to the infinite slit approximation where the far ends of the slit are neglected. When performing a 2D simulation of a slit array, the domain represents a cross-sectional profile of the actual slit, as shown in Figure 2. Its geometry fully determined by the
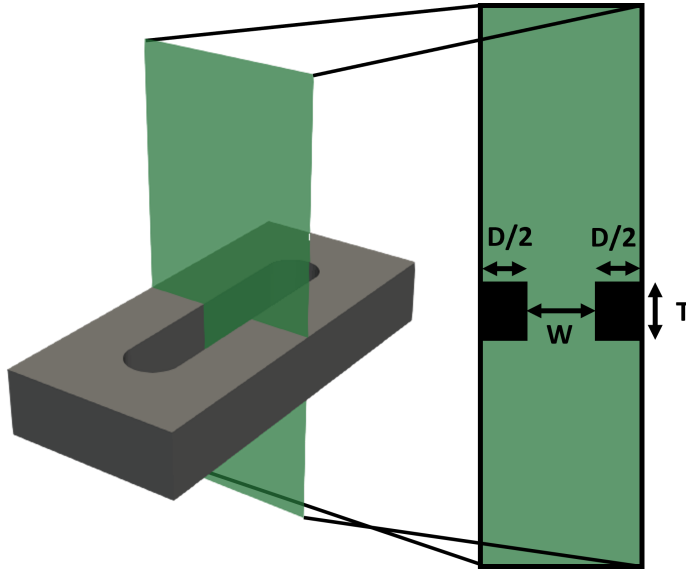

Figure 2: Visualization of the 2D configuration.

width W, the spacing between adjacent slits D, and the plate thickness T.

In two dimensions, the porosity is defined as $W/(D+W)$. The question we aim to address is: What length does the actual 3D slit need to have to be accurately represented by a 2D configuration?

To answer this question, a preliminary study is carried out by comparing the results obtained from a 2D simulation with those of 3D simulations of slits with increasing length. The burner temperature is chosen as the test quantity for this analysis due to its significant impact on flashback [34]. Both 2D and 3D simulations are performed at $\phi = 0.6$ with a fixed inlet velocity corresponding to $V_{\mathrm{S}} = 4\,\mathrm{m/s}$. In all cases, the plate thickness is $T = 0.6\,\mathrm{mm}$, the slit width is $W = 0.5\,\mathrm{mm}$, and the distance between two adjacent slits is $D = 1\,\mathrm{mm}$. For the 3D simulations, the length L is varied in the range 1-50 mm. The burner temperature as a function of the slit length, along with the results of the 2D case, is shown in Figure 3. The 2D simulation predicts
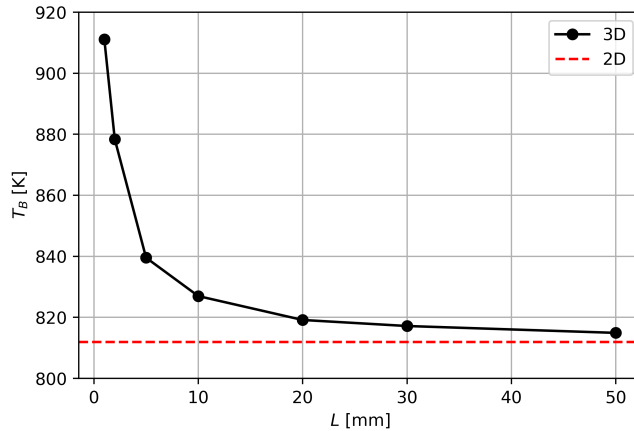

Figure 3: Burner plate temperature as a function of the slit length for $W = 0.5\,\mathrm{mm}$ and $D = 1\,\mathrm{mm}$. The red dashed line represents the 2D result.

a burner temperature of $T_B = 812\,\mathrm{K}$. In contrast, 3D simulations predict a

12

higher burner temperature of $T_B = 911\,\text{K}$ for $L = 1\,\text{mm}$, which decreases to $T_B = 826\,\text{K}$ when $L = 10\,\text{mm}$, ultimately converging with the 2D result as L approaches $50\,\text{mm}$. Higher burner temperatures for shorter slits can be readily explained by an increasing impact of the slit extremities, where additional heat is transferred from the flame to the burner plate. As the length is increased, the relative impact of the extremity regions decreases, until the 2D result, for which these regions are completely neglected, is recovered.

The findings from this preliminary analysis highlight the inadequacy of the infinite slit approximation for slits shorter than $50\,\text{mm}$. Considering that slits in practical devices are usually much shorter than $50\,\text{mm}$, 2D configurations prove to be inadequate representations of the actual geometry. This underscores the necessity of utilizing 3D simulations to accurately capture the behavior of practical devices, accounting for the complete geometric complexity of the slit configuration, and motivates a thorough analysis of the influence of the third dimension on flashback limits.

4.2. Effect of the slit length

To analyze the effect of the third dimension on the flashback limits, we compute the flashback velocities at three equivalence ratios, $\phi = 0.6$, 0.8, and 1.0, for slits with different lengths. The considered values of L are $L = 0\,\text{mm}$ (circular hole), $0.5\,\text{mm}$, $1\,\text{mm}$, $2\,\text{mm}$, $4\,\text{mm}$, and $8\,\text{mm}$. Longer slits are not investigated because they are not practically relevant for real burners. For all cases, a fixed porosity of $A_{\text{slit}}/A_{\text{tot}} = 0.2$ is imposed by adjusting D. In Figure 4 we plot V_{FB} versus L for various equivalence ratios. Both unnormalized and normalized values are presented in panels (a) and (b), respectively. The flashback velocity and the slit length are scaled with the 1D unstretched

13

laminar flame speed s_L and thermal flame thickness δ_T, respectively. Additionally, we include the flashback velocity computed for a 2D configuration representing an infinite slit with the same width and porosity imposed for 3D cases, corresponding to $W = 0.5\,\text{mm}$ and $D = 2\,\text{mm}$. As expected, V_{FB}
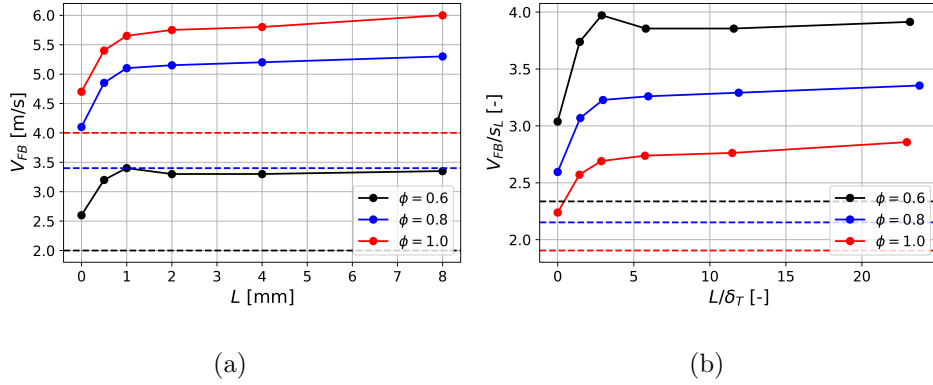

(a)   (b)

Figure 4: Flashback velocity plotted against slit length for various equivalence ratios: (a) non-normalized values and (b) normalized values with respect to s_L and δ_T. 2D results are indicated by dashed horizontal lines.

increases with an increase in the equivalence ratio due to a higher laminar flame speed. Conversely, the normalized flashback velocity V_{FB}/s_L, which is a more reliable indicator of the flashback propensity as it removes the trivial dependence on the laminar flame speed, exhibits the opposite trend. As flashback of hydrogen flames is strongly influenced by preferential diffusion effects, a higher flashback propensity for leaner mixtures is expected [33, 36]. The flashback velocity increases rapidly between $L = 0\,\text{mm}$ and $L = 1\,\text{mm}$. However, for $L > 1\,\text{mm}$, the dependence of the flashback velocity on the slit length diminishes significantly. This observation suggests a distinct behavior of circular holes and very short slits compared to longer slits, which exhibit a consistent behavior irrespective of their length. The 2D results exhibit sig-

14

nificant deviations from the 3D results, with the latter being approximately 1.5 times higher. Notably, unlike the observed behavior of the burner plate temperature in Figure 3, the 3D results for the flashback velocity do not converge to the 2D values for large slit lengths.

To understand the distinct behaviors of the circular hole configuration and the slit configuration, we investigate the differences in the flame structure at the flashback limits for the circular hole and a slit. In Figures 5 and 6, we show temperature, local equivalence ratio, and normalized H_2 consumption rate profiles for the circular hole configuration and the slit with length $L = 2\,\mathrm{mm}$ (transverse and longitudinal section) at the flashback limit, for the case $\phi = 0.6$. The local equivalence ratio φ is defined using the Bilger formula [37] and normalized with the mixture equivalence ratio $\phi_{\mathrm{in}} = 0.6$. The molecular H_2 consumption rate ω_{H_2} is normalized as $\bar{\omega}_{H_2} = \omega_{H_2}/\max(\omega_{H_2,\mathrm{1D}})$, where $\max(\omega_{H_2,\mathrm{1D}})$ is the maximum H_2 consumption rate obtained for the corresponding unstretched 1D flame. To visualize the flame front, iso-contours of progress variable are plotted. The progress variable is defined as $C = 1 - Y_{H_2}/Y_{H_2,u}$, where Y_{H_2} denotes the mass fraction of H_2, and $Y_{H_2,u}$ represents its value in the unburnt mixture. For the circular hole, we observe the flame front to be very close to the hole exit. The flame thickness is comparable with the radius of the hole, and the flame is attached both at the top and the inner sides of the burner plate. The enclosed geometry leads to high pre-heating of the fresh gases, caused by the heating of the flow when passing through the hot hole: the heat lost by the flame to the burner at the top of the plate is given back to the flow on the bottom and the inner sides of the plate, causing the gases to be preheated
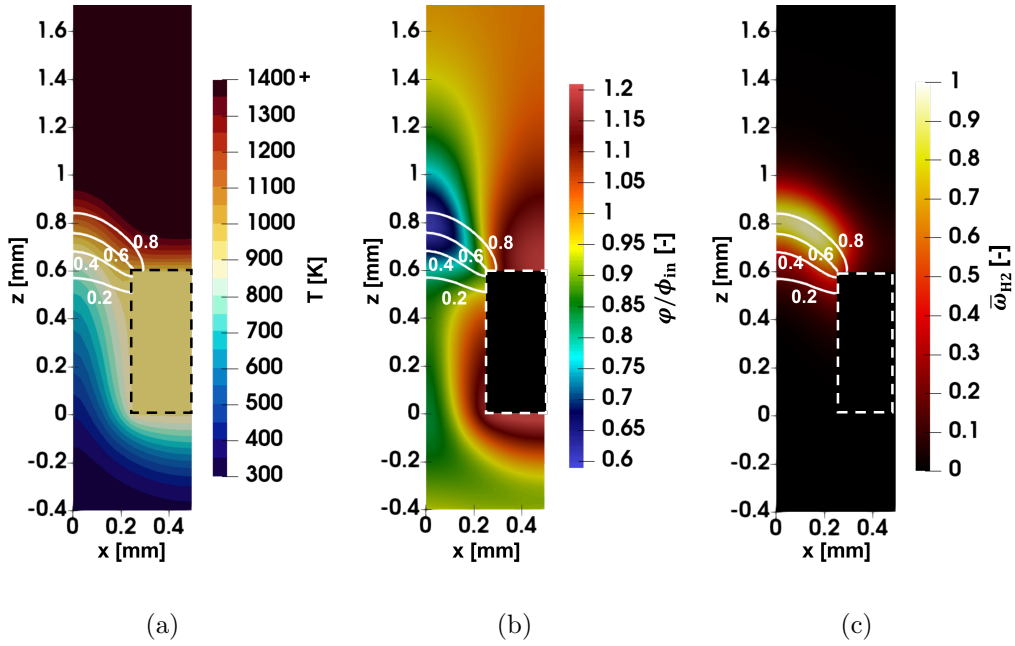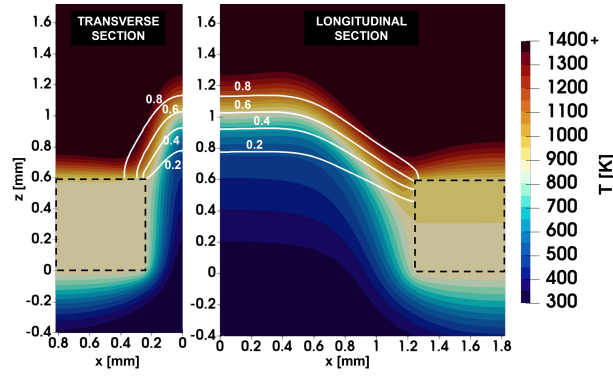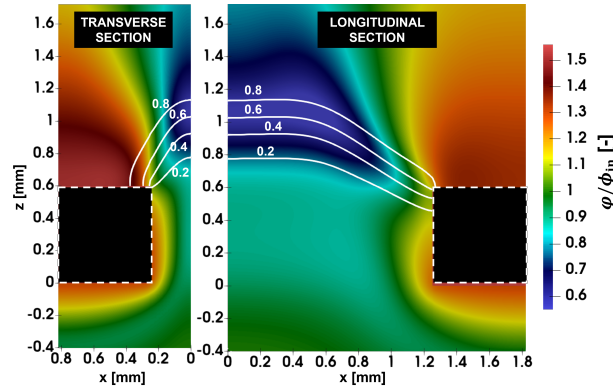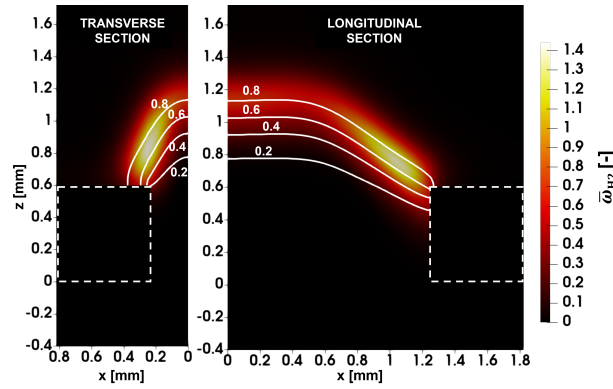
15

Figure 5: (a) Temperature, (b) normalized equivalence ratio, and (c) normalized H_2 consumption rate profiles for the circular hole at the flashback limit for the case $\phi = 0.6$. Progress variable iso-contours are plotted in white. The solid zone representing the burner plate is delimited by the dashed line.

16

Figure 6: (a) Temperature, (b) normalized equivalence ratio, and (c) normalized H_2 consumption rate profiles for the slit with length $L = 2\,\text{mm}$ at the flashback limit for the case $\phi = 0.6$. Progress variable iso-contours are plotted in white. The solid zone representing the burner plate is delimited by a dashed line.

when reaching the flame front. Due to the small width of the channel, the mixture temperature is approximately uniform when reaching the flame zone, with $T \simeq 800\,\mathrm{K}$ at $C = 0.2$. In Figure 5(b) we observe variations in the local equivalence ratio caused by preferential diffusion. Two sources of preferential diffusion are observed: one induced by the flame front curvature and the other by Soret diffusion. For mixtures with effective Lewis numbers smaller than one, preferential diffusion effects cause φ to be reduced at the tip of the flame due to negative curvature, leading to the enrichment of the flame base region [43]. Additionally, Soret diffusion causes light species like H_2 to diffuse toward hotter regions in the presence of temperature gradients, leading to the enrichment of the mixture close to the hot burner plate [19]. However, for the circular hole, no significant enrichment is observed in the flame region. The shape of the flame is approximately hemispherical, suppressing curvature-induced preferential diffusion effects. Moreover, no significant Soret-induced enrichment is observed at the flame base. This flame configuration suggests that the main mechanism driving the flashback is the pre-heating of the unburnt gases: despite the flow velocity increasing with its temperature due to a decrease in density, the flame speed increases faster than linearly with the unburnt mixture temperature [41]. When the inlet velocity is decreased, the flame finds a new stable position, closer to the burner plate, further increasing the solid temperature and the pre-heating of the mixture. When a critical inlet velocity and a critical temperature are reached, the flame speed surpasses the bulk velocity, causing the flame to flashback into the hole.

Conversely, in the case of the slit, a significantly more pronounced influence of preferential diffusion is observed. The elongated shape of the slit

induces non-uniformities in the curvature of the flame front, resulting in the enrichment of the mixture in the flame base regions along both the sides of the slit and its extremities. Additionally, the presence of temperature gradients pushes the fuel toward the hot burner plate surface due to the Soret effect, causing further enrichment in the flame base region. As a consequence of these two effects, a peak of $\bar{\omega}_{H_2} \simeq 1.5$ is observed at the flame base. Mixture pre-heating is more prominent near the far end, where the enclosed geometry promotes heat transfer. Consequently, due to an enhanced flame speed, the flame stabilizes further upstream in comparison to the slit side, attaching to the inner wall of the burner plate. This positioning designates this region as the likely initiation zone for flashback: if the heightened flame speed, resulting from both increased H_2 consumption rates and mixture pre-heating, exceeds the flow velocity in the critical region near the wall, where the flow velocity is low, flashback is initiated.

The crucial role of the slit extremities in initiating the flashback also accounts for the disparities between 2D and 3D results illustrated in Figure 4. The flashback limits computed for 3D configurations do not converge to the 2D values for long slits, indicating intrinsically different flashback mechanisms for the two configurations. To gain deeper insights into this observation, the analysis of the flashback dynamics in 3D configurations is particularly valuable.

4.3. Flashback dynamics

In this section, we analyze the flashback dynamics occurring in a three-dimensional slit. To do this, we make use of the transient simulation for a slit with $L = 2\,\mathrm{mm}$ at $\phi = 0.6$ described in Section 3. Transient simulations

provide the opportunity to observe the flashback dynamics, which is not possible using the steady-state approach.

Figure 7 depicts a sequence of three snapshots captured during the last stage of the simulation. The snapshots illustrate the evolution of the flame front after the reduction of the inlet velocity from the last stable velocity to the flashback velocity. An iso-surface of progress variable, corresponding to $C = 0.3$, is plotted to identify the flame front. The initial instant, denoted as $t = 0$, marks the moment of the reduction of the inlet velocity. At $t = 0$, the flame front is in its initial stable position (Figure 7 (a)). During the first 40 ms, we observe minimal alterations in the flame front position. By $t = 40$ ms, flashback initiates rapidly within the slit (Figure 7 (b)). The initiation is asymmetric and originates at the ends of the slit. Here, the flame front moves backward towards the entrance of the slit, traversing it entirely on that side (Figure 7 (c)), ultimately driving the entire flashback process (Figure 7 (d)). For a better visualization of the important physical mechanisms involved, a colored 3D visualization of the last stable flame, corresponding to Figure 7 (a), is shown in Figure 8. The iso-contour of progress variable corresponding to $C = 0.3$ is colored by temperature (a), normalized local equivalence ratio (b), and normalized molecular H_2 consumption rate (c). A temperature peak is observed at the slit far ends, where the enclosed geometry promotes heat transfer, leading to higher pre-heating (Figure 8(a)). Preferential diffusion effects, driven by curvature and Soret effect, induce the enrichment of the mixture in the same regions. Both of these phenomena contribute to an increase in the H_2 consumption rate (Figure 8 (c)), and a subsequent increase in the flame speed. Consequently, this region emerges as
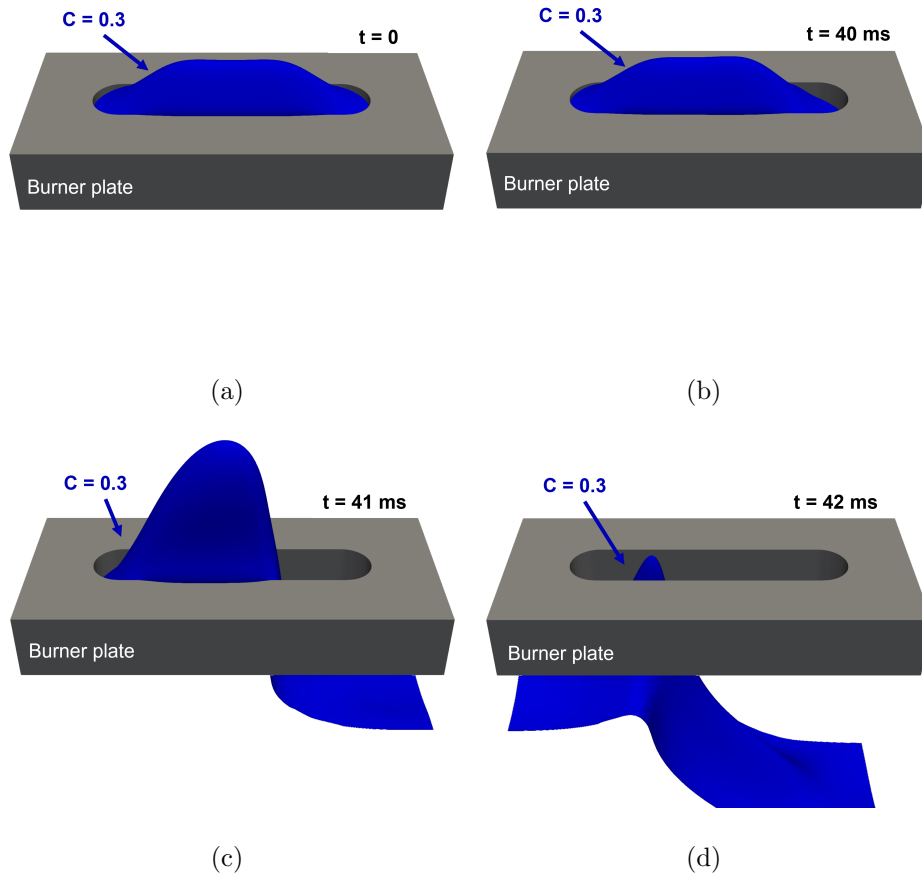
20

Figure 7: Snapshots of the transient simulation for the slit with $L = 2\,\text{mm}$, corresponding to four instants during the occurrence of flashback. Iso-surfaces of progress variable at $C = 0.3$ are shown to visualize the flame front. The burner plate geometry is included as a reference. $t = 0$ marks the moment of the reduction of the inlet velocity from the last stable velocity to V_{FB}.
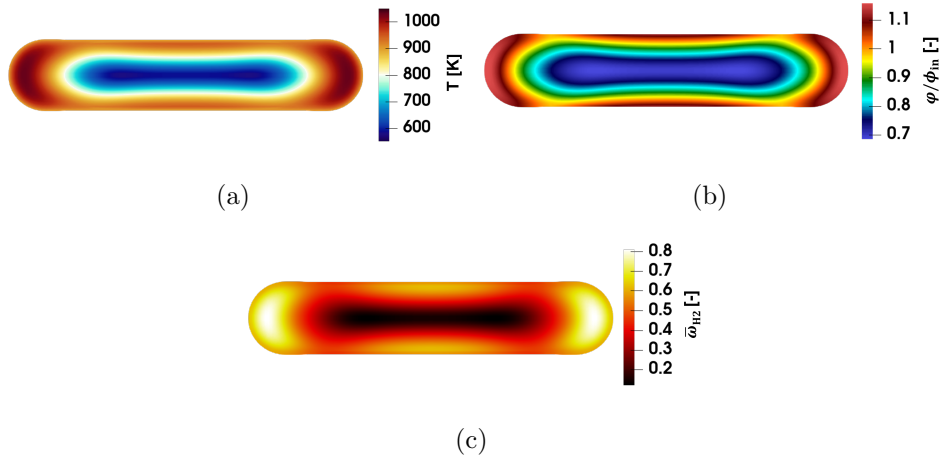
Figure 8: Iso-contour of progress variable $C = 0.3$ for a slit with $L = 2\,\mathrm{mm}$ at the flashback limit for the case $\phi = 0.6$ (top view). The iso-contours are colored by: (a) temperature, (b) normalized local equivalence ratio, and (c) normalized H_2 consumption rate.

the flashback initiation zone, with the local flame speed exceeding the flow velocity and triggering flashback.

The observation of this distinctive dynamics explains the weak dependence of the flashback velocity on the length of the slit above a certain value (Figure 4), as we anticipate the critical region for flashback initiation to be consistently located at the ends of the slit, irrespective of the specific value of L. Furthermore, the crucial role played by the slit extremities makes flashback an intrinsically three-dimensional phenomenon, with enhanced preheating in these regions causing the initiation of flashback at higher inlet velocities compared to 2D configurations. In 2D, flashback is initiated when the imbalance between the flow velocity and the flame speed is reached at the sides of the slit [33–36], and this occurs at lower inlet velocities. Consequently, the 3D results in Figure 4 do not converge to those obtained in 2D

configurations, where the slit extremities are consistently neglected.

5. Conclusions

In this study, we investigated the influence of the three-dimensional geometry of the slits on the flashback limits of hydrogen-premixed flames in perforated burners. We conducted steady-state and transient simulations to compute the flashback limits for slits with varying lengths and compared the results with those obtained in 2D configurations. Furthermore, we performed transient simulations to investigate the three-dimensional flashback dynamics.

A preliminary analysis was conducted to estimate the range of applicability of the infinite slit approximation, commonly employed in 2D simulations used in the literature for flashback velocity estimations. We computed the burner plate temperature, chosen as the test quantity, for a given inlet velocity in three-dimensional slits with increasing length and in a 2D configuration. Our results highlighted the inadequacy of the infinite slit approximation, as the 3D results converged to the 2D ones only for slit lengths beyond practical interest.

Flashback limits were computed for slits with fixed width and increasing length, ranging from $L = 0$ (corresponding to a circular hole) to $L = 8\,\mathrm{mm}$. The circular hole was found to be more resistant to flashback, due to weaker preferential diffusion effects compared to the slits. However, for $L > 0$, the flashback velocity was found to exhibit a weak dependence on the slit length. The results were compared with the flashback velocity obtained in a 2D configuration. Notably, in this case, the 3D results do not converge to those

obtained in 2D configurations for large L, and the 2D results were found to significantly underestimate the flashback velocity.

The flashback dynamics in a slit was investigated in detail using transient simulations. The flashback was found to be initiated asymmetrically at one extremity of the slit, where the imbalance between the flame speed and the flow velocity causes the flame front to move upstream, ultimately driving the entire flashback process. The location of the initiation of the flashback is due to two combined mechanisms. Firstly, mixture enrichment is observed at the flame base in the slit extremities region due to curvature-induced preferential diffusion and the Soret effect. Furthermore, the enclosed geometry of the slit far ends promotes the heat transfer from the hot burner plate to the fresh mixture, increasing its pre-heating. Both these effects increase the flame speed in that critical zone, triggering the initiation of flashback. This observation explains the weak dependence of the flashback velocity on the length of the slit, as we anticipate the critical region for flashback initiation to be consistently located at the ends of the slit, irrespective of the specific value of L. Furthermore, the crucial role played by the slit extremities explains why the 3D results do not converge to those obtained in 2D configurations, where the slit extremities are always neglected.

Author contributions

Acknowledgements

24

"Research and Innovation" resources - Green/Innovation Action - DM MUR 1061/2021 and DM MUR 1062/2021.

References

[1] S. van Renssen, The hydrogen solution?, Nature Climate Change 10 (9) (2020) 799–801.

[2] R. Winkler-Goldstein, A. Rastetter, Power to gas: The final breakthrough for the hydrogen economy?, Green 3.

[3] R. McKenna, Q. Bchini, J. Weinand, J. Michaelis, S. König, W. Köppel, W. Fichtner, The future role of power-to-gas in the energy transition: Regional and local techno-economic analyses in baden-württemberg, Appl. Energy 212 (2018) 386–400.

[4] J. Michalski, U. Bünger, F. Crotogino, S. Donadei, G.-S. Schneider, T. Pregger, K.-K. Cao, D. Heide, Hydrogen generation by electrolysis and storage in salt caverns: Potentials, economics and systems aspects with regard to the german energy transition, Int. J. Hydrog. Energy 42 (19) (2017) 13427–13443.

[5] M. Najarnikoo, M. Z. Targhi, H. Pasdarshahri, Experimental study on the flame stability and color characterization of cylindrical premixed perforated burner of condensing boiler by image processing method, Energy 189 (2019) 116130.

[6] R. Lamioni, C. Bronzoni, M. Folli, L. Tognotti, C. Galletti, Impact of H2-enriched natural gas on pollutant emissions from domestic condens-

25

ing boilers: numerical simulations of the combustion chamber, Int. J. Hydrog. Energy 48 (51) (2023) 19686–19699.

[7] R. Lamioni, C. Bronzoni, M. Folli, L. Tognotti, C. Galletti, Effect of slit pattern on the structure of premixed flames issuing from perforated burners in domestic condensing boilers, Combustion Theory and Modelling 27 (2) (2023) 218–243.

[8] F. Schiro, A. Stoppato, Experimental investigation of emissions and flame stability for steel and metal fiber cylindrical premixed burners, Combustion Science and Technology 191 (3) (2019) 453–471.

[9] J. Edacheri Veetil, B. Aravind, A. Mohammad, S. Kumar, R. K. Velamati, Effect of hole pattern on the structure of small scale perorated plate burner flames, Fuel 216 (2018) 722–733.

[10] C. Smith, J. Mouli-Castillo, D. van der Horst, S. Haszeldine, M. Lane, Towards a 100barriers to the first demonstrator project in the united kingdom, Int. J. Hydrog. Energy 47 (55) (2022) 23071–23083.

[11] Y. Zhao, V. McDonell, S. Samuelsen, Influence of hydrogen addition to pipeline natural gas on the combustion performance of a cooktop burner, Int. J. Hydrog. Energy 44 (23) (2019) 12239–12253.

[12] H. de Vries, H. B. Levinsky, Flashback, burning velocities and hydrogen admixture: Domestic appliance approval, gas regulation and appliance development, Appl. Energy 259 (2020) 114116.

[13] X. Wu, H. Zhang, M. Yang, W. Jia, Y. Qiu, L. Lan, From the perspective of new technology of blending hydrogen into natural gas pipelines

transmission: Mechanism, experimental study, and suggestions for further work of hydrogen embrittlement in high-strength pipeline steels, Int. J. Hydrog. Energy 47 (12) (2022) 8071–8090.

[14] A. L. Sánchez, F. A. Williams, Recent advances in understanding of flammability characteristics of hydrogen, Progress in Energy and Combustion Science 41 (2014) 1–55.

[15] L. Berger, A. Attili, H. Pitsch, Intrinsic instabilities in premixed hydrogen flames: Parametric variation of pressure, equivalence ratio, and temperature. part 1 - dispersion relations in the linear regime, Combust. Flame 240 (2022) 111935.

[16] W. Zhang, J. Wang, W. Lin, R. Mao, H. Xia, M. Zhang, Z. Huang, Effect of differential diffusion on turbulent lean premixed hydrogen enriched flames through structure analysis, Int. J. Hydrog. Energy 45 (18) (2020) 10920–10931.

[17] K. S. Kedia, A. F. Ghoniem, Mechanisms of stabilization and blowoff of a premixed flame downstream of a heat-conducting perforated plate, Combust. Flame 159 (3) (2012) 1055–1069.

[18] F. Vance, Y. Shoshin, J. van Oijen, L. de Goey, Effect of lewis number on premixed laminar lean-limit flames stabilized on a bluff body, Proc. Combust. Inst. 37 (2) (2019) 1663–1672.

[19] F. H. Vance, P. de Goey, J. A. van Oijen, The effect of thermal diffusion on stabilization of premixed flames, Combust. Flame 216 (2020) 45–57.

27

[20] Z. Wang, X. Han, Y. He, S. Wang, R. Ji, Y. Zhu, K. Cen, Investigation of flame and burner plate interaction during the heat flux method used for laminar burning velocity measurement, Fuel 266 (2020) 117051.

[21] W. Jin, C. Ren, J. Li, J. Wang, Y. Yan, Experimental study on characteristics of CH_4/H_2 oxy-fuel turbulent premixed flames, Fuel 310 (2022) 122292.

[22] V. Kurdyumov, E. Fernández-Tarrazo, J.-M. Truffaut, J. Quinard, A. Wangher, G. Searby, Experimental and numerical study of premixed flame flashback, Proc. Combust. Inst. 31 (1) (2007) 1275–1282.

[23] T. B. Kıymaz, E. Böncü, D. Güleryüz, M. Karaca, B. Yılmaz, C. Allouis, İskender Gökalp, Numerical investigations on flashback dynamics of premixed methane-hydrogen-air laminar flames, Int. J. Hydrog. Energy 47 (59) (2022) 25022–25033.

[24] K. S. Kedia, A. F. Ghoniem, The blow-off mechanism of a bluff-body stabilized laminar premixed flame, Combust. Flame 162 (4) (2015) 1304–1315.

[25] H. M. Altay, K. S. Kedia, R. L. Speth, A. F. Ghoniem, Two-dimensional simulations of steady perforated-plate stabilized premixed flames, Combustion Theory and Modelling 14 (1) (2010) 125–154.

[26] H. Xia, W. Han, X. Wei, M. Zhang, J. Wang, Z. Huang, C. Hasse, Numerical investigation of boundary layer flashback of CH4/H2/air swirl flames under different thermal boundary conditions in a bluff-body swirl burner, Proc. Combust. Inst. 39 (4) (2023) 4541–4551.

[27] D. Ebi, N. T. Clemens, Experimental investigation of upstream flame propagation during boundary layer flashback of swirl flames, Combust. Flame 168 (2016) 39–52.

[28] R. Ranjan, N. T. Clemens, Insights into flashback-to-flameholding transition of hydrogen-rich stratified swirl flames, Proc. Combust. Inst. 38 (4) (2021) 6289–6297.

[29] H. de Vries, A. V. Mokhov, H. B. Levinsky, The impact of natural gas/hydrogen mixtures on the performance of end-use equipment: Interchangeability analysis for domestic appliances, Appl. Energy 208 (2017) 1007–1019.

[30] A. Aniello, T. Poinsot, L. Selle, T. Schuller, Hydrogen substitution of natural-gas in premixed burners and implications for blow-off and flashback limits, Int. J. Hydrog. Energy.

[31] H. Pers, A. Aniello, F. Morisseau, T. Schuller, Autoignition-induced flashback in hydrogen-enriched laminar premixed burners, Int. J. Hydrog. Energy.

[32] F. Vance, Y. Shoshin, L. de Goey, J. van Oijen, Quantifying the impact of heat loss, stretch and preferential diffusion effects to the anchoring of bluff body stabilized premixed flames, Combust. Flame 237 (2022) 111729.

[33] F. Vance, L. de Goey, J. van Oijen, Development of a flashback correlation for burner-stabilized hydrogen-air premixed flames, Combust. Flame 243 (2022) 112045.

[34] F. Fruzza, R. Lamioni, L. Tognotti, C. Galletti, Flashback of H2-enriched premixed flames in perforated burners: Numerical prediction of critical velocity, Int. J. Hydrog. Energy 48 (81) (2023) 31790–31801.

[35] E. Flores-Montoya, A. Aniello, T. Schuller, L. Selle, Predicting flashback limits in H2 enriched CH4/air and C3H8/air laminar flames, Combust. Flame 258 (2023) 113055.

[36] F. Fruzza, R. Lamioni, A. Mariotti, M. V. Salvetti, C. Galletti, Preprint: Flashback propensity due to hydrogen blending in natural gas: sensitivity to operating and geometrical parameters (2023). `doi:https://doi.org/10.48550/arXiv.2311.18441`.

[37] R. Bilger, S. Stårner, R. Kee, On reduced mechanisms for methane-air combustion in non-premixed flames, Combust. Flame 80 (2) (1990) 135–149.

[38] Ansys Inc, Ansys Fluent 22.1 User's guide (2022).

[39] W. E. Stewart, Multicomponent mass transfer., AIChE J. 41 (1) (1995) 202–203.

[40] H. J. Merk, The macroscopic equations for simultaneous heat and mass transfer in isotropic, continuous and closed systems, Appl. Sci. Res., Sec. A 8 (1) (1959) 73–99.

[41] K. Kuo, Principles of Combustion, Wiley, 2005.

[42] M. Modest, Radiative Heat Transfer, Elsevier Science, 2013.

[43] C. Law, Dynamics of stretched flames, Symp. Combust. Proc. 22 (1) (1989) 1381–1402.